Journal of Molecular Structure 1040 (2013) 39–46

Contents lists available at SciVerse ScienceDirect

Journal of Molecular Structure

journal homepage: www.elsevier.com/locate/molstruc

ESR and magnetic studies of octahedral [Fe(III)(Cl)(pcd)(H_2O)(DMSO)] (pcd = pyridine-2,6-dicarboxylato) compound showing Fe(III) species with different spin states in solution

Samuel Hernández-Anzaldo [a], Nailea Sánchez-Morales [a], Rafael Zamorano-Ulloa [b], Roberto Escudero [c], María de Jesús Rosales Hoz [d], Yasmi Reyes-Ortega [a,*]

[a] Centro de Química, Instituto de Ciencias, Universidad Autónoma de Puebla, Edif. 103F, CU, San Manuel, 72570 Puebla, Pue., Mexico
[b] Departamento de Física, ESFM, IPN, Av. Instituto Politécnico Nacional S/N, Edif. 9, U.P. Zacatenco, Col. San Pedro Zacatenco, 07738 México, DF, Mexico
[c] Instituto de Investigaciones en Materiales, UNAM, A. Postal 70-360, 04510 México, DF, Mexico
[d] Departamento de Química, CIVESTAV, IPN, Av. Instituto Politécnico Nacional 2508, San Pedro Zacatenco, C.P. 07360 México, DF, Mexico

HIGHLIGHTS

- We have proved the correlation between Fe(III)-spin-state and peroxidase activity.
- ESR spectra of solution samples show species with different iron(III) spin state.
- By ESR spectrometry it has been identified quantum mixes S = 3/2, S = 5/2 of Fe(III).
- Structural analyses is consistent with Fe(III) antiferromagnetic exchange interaction.

ARTICLE INFO

Article history:
Received 11 April 2012
Received in revised form 14 December 2012
Accepted 11 February 2013
Available online 26 February 2013

Keywords:
Fe(III) supramolecular structure
Quantum mixed spin state $^3/_2$ $^5/_2$
High spin $^5/_2$
Low spin ½
Magnetic studies
Catalytic activity

ABSTRACT

By direct synthesis has been obtained the octahedral complex [Fe(III)(Cl)(pdc)(H_2O)(DMSO)] **1** (pdc = pyridyn-2,6-dicarboxylato), which shows a supramolecular structure and a clear and large molecular distortion. UV–Vis spectrum of **1** shows at 741 nm, 836 nm ($\varepsilon = 100\ M^{-1}\ cm^{-1}$) and 970 nm ($\varepsilon = 1600\ M^{-1}\ cm^{-1}$) typical iron d–d transitions. FIR spectrum of **1** shows vibrations υ_{Fe-O}, υ_{Fe-N} and υ_{Fe-Cl}. NMR ^1H spectroscopy is typical of paramagnetic compounds. The susceptibility data fit to a Hamiltonian, $H_{ex} = -2JS_1 \cdot S_2$, using two models, give close exchange interaction constant values of: $J = -1.803\ cm^{-1}$, $g = 1.810$ and $J = -1.102\ cm^{-1}$, $g = 1.832$. X-band ESR spectra of powder sample of **1** at 300 K/77 K show broad signals at $H \approx 56.70$ mT/64.53 mT, characteristic of ferromagnetic absorptions. X-band spectra of **1** at 77 K in methanol solution at different concentrations show typical signals of Fe(III) species with high spin, $S = {}^5/_2$, quantum mixed spin state (qms), $^5/_2$, $^3/_2$, which are present in ESR spectra of peroxidase enzymes, and a low spin $S = {}^1/_2$. **1** has been used as catalyst in the guaiacol test, characteristic of peroxidase enzymes, giving positive by visual observation and by UV–Vis spectroscopy. By ERS spectroscopy has been observed the characteristic π-cationic-radical ferryl, enzyme covalently modified, when the peroxidase enzyme is active. The presence of Fe(III) species with qms observed by ESR spectra of **1**, and its catalytic activity, both characteristic of peroxidase enzymes, are a significant conclusion of the work.

1. Introduction

Many compounds containing Fe(III) exhibit only Fe(III) $^5/_2$ or $^1/_2$ pure spin sates but, it has been observed too the thermal mixed spin state $S = {}^1/_2$, $^5/_2$, and the quantum mixed spin state $^3/_2$, $^5/_2$, as ground state [1–5]. Ferric hemeproteins show, likewise, species of iron(III) with quantum mix spin state (qms), $S = {}^3/_2$, $S = {}^5/_2$ [1,2]. ESR, magnetic susceptibility and Mössbauer studies of hemeproteins and iron(III) compounds, have shown that pure spin state of iron(III) $S = {}^3/_2$ is not common and this spin state appears as quantum mixed spin state $^3/_2$, $^5/_2$, which proportion of $S = {}^3/_2$ spin state of iron(III) in qms, $S = {}^3/_2$, $S = {}^5/_2$, vary depending on the iron(III) coordination sphere [3–10]. However, there is a big difficulty to crystallize both, as ferric hemeproteins as their model compounds, porphyrins–Fe(III) complexes, and also it is a challenge to predict other iron(III) complexes with these, above mention, spin states by theoretical calculus [9–14]. It is important to note that it is necessary to know

* Corresponding author.
E-mail address: yasmi.reyes@correo.buap.mx (Y. Reyes-Ortega).

0022-2860/$ - see front matter © 2013 Elsevier B.V. All rights reserved.
http://dx.doi.org/10.1016/j.molstruc.2013.02.021

molecular geometries to carry out quantum chemical calculations to oversee molecular properties starting from these geometries [11–15]. The ESR spectra of **1** in methanol solution at ca ⩽ 23 mM show that the supramolecular structure is destroyed and different monomer of Fe(III) are formed, some of the ESR signals are typical of species with high spin $S = {}^5/_2$, some corresponding at low spin $S = ½$, and some at qms $S = {}^3/_2$, $S = {}^5/_2$. Studies on the correlation between qms of porphyrin–Fe(III) compounds models of peroxidase enzymes and their catalytic activity have been reported [9–11]. However, we do not find reports of other type of Fe(III) complexes, different to these porphyrin–Fe(III) derivatives, which have used as catalysts-peroxidase. In this work we are reporting the direct synthesis [16–19] using metallic Fe and pcd ligand (pdc = 2,6-pyridyndicarboxylato) to obtain [Fe(III)(Cl)(pdc)(H_2O)(DMSO)] **1**, its electronic and magnetic studies, and its catalytic activity, qualitatively, using the guaiacol test, characteristic of peroxidase enzyme [20]. It is important to emphasize that **1** structure has been reported by Rafizadeh et al. [21], whom prepared it by traditional synthesis method using the ion and the pcd ligand, and this structure is analogous at that obtained for us.

2. Experimental section

2.1. Crystal structure determination

Relevant crystallographic data are presented in Table 1. A crystal, 0.30 × 0.20 × 0.05 mm^3, was mounted on an Enraf–Nonius CCD diffractometer at 293(2) K, following a standard procedure [22]. A total of 9015 unique reflection intensities were measured in the range $4.56 < 2\theta < 54.96°$. Corrections were made for Multi-Scans for absorption correction (transmission ranges: 0.9282 and 0.6597). The structure was solved by direct methods and refined by full-matrix least-squares techniques with anisotropic temperature factors for the non-H atoms. Maximum differences peak in the final σF map was 0.281 e $Å^{-3}$. Maximum Δ/σ in the last cycle was 0.000. Goodness of fit was 1.023. Calculations were made with SHELX 97 [23]. Relevant geometric parameters are given in Table 2. Complete data were deposited as a CIF file (deposition number: CCDC 800579). Structure factors and raw files are available on request.

2.2. General methods

Electronic spectrum is recorded in a Shimadzu UV/VIS/NIR 3100 spectrophotometer on ca 0.001 mM methanol sample solution, at 300 K, using cells with 1 cm path length. A Nicolet Magna-IR 750 spectrophotometer is employed to record the infrared spectrum using KBr pellets. The ^{1}H NMR spectrum is recorded at 25 °C on a Varian MERCURY 300 spectrometer, using methanol-*d* solutions with ca 10 mM. The ^{1}H NMR spectrum is obtained from 100 ppm to −100 ppm with 150 repetitions. ESR spectra at X-band frequencies are obtained at variable temperature (300–77 K) with a JEOL JES-RES 3X spectrometer on polycrystalline powder sample, and in CH_3OH solutions at 10 different concentrations from 0.028 M to 0.003 M. Magnetic measurements are performed on a Quantum Design Magnetometer MPMS-5S, with a precision of 10^{-8} emu, and different magnetic intensities in the range of temperatures from 2 to 300 K. The electronic impact (EI) ionization mass spectra and high resolution mass spectra (FAB+) are acquired on a JEOL MStation JMS-700 mass spectrometer. Catalytic activity of has been carried out as previously for pinch-porphyrin–Fe(III) reported [9,10].

Table 1
Bond lengths (Å) and angles (°).

Bond lenghts			
C(1)—O(6)	1.229(3)	C(1)—O(3)	1.287(3)
C(7)—O(4)	1.280(3)	C(8)—S(1)	1.772(3)
C(9)—S(1)	1.774(3)	O(1)—Fe(1)	2.039(2)
O(1)—S(2)	1.544(39	O(2)—Fe(1)	2.015(2)
O(3)—Fe(1)	2.0200(19)	O(4)—Fe(1)	2.0537(19)
Cl(1)—Fe(1)	2.2663(10)	Fe81)—N(1)	2.082(2)
Angles			
O(6)—C(1)—O(3)	126.0(3)	O(6)—C(1)—C(2)	120.1(3)
N(1)—C(2)—C(3)	121.0(2)	O(5)—C(7)—O(4)	124.9(3)
S(1)—O(2)—Fe(1)	118.96(12)	C(1)—O(3)—Fe(1)	120.46(17)
O(6)—C(1)—O(3)	92.31(8)	O(2)—Fe(1)—O(1)	174.58(8)
O(3)—Fe(1)—O(1)	91.86(8)	O(2)—Fe(1)—O(4)	88.05(8)
O(3)—Fe(1)—O(4)	151.34(8)	O(1)—Fe(1)—O(4)	86.63(8)
O(2)—Fe(1)—N(1)	89.65(9)	O(3)—Fe(1)—N(1)	75.91(8)
O(1)—Fe(1)—N(1)	88.00(9)	O(4)—Fe(1)—N(1)	75.43(8)
O(2)—Fe(1)—Cl(1)	91.45(7)	O(3)—Fe(1)—Cl(1)	102.71(6)
O(1)—Fe(1)—Cl(1)	91.01(7)	O(4)—Fe(1)—Cl(1)	105.94(6)
N(1)—Fe(1)—Cl(1)	178.27(7)	C(2)—N(1)—C(6)	122.6(2)
C(2)—N(1)—Fe(1)	118.41(17)	C(6)—N(1)—Fe(1)	119.00(18)

2.3. Catalytic activity

Determination of guaiacol oxidation with hydrogen peroxide using **1** as catalyst is carried out as previously described for horseradish peroxidase [20]. Formation guaiacol oxidation products (POG) are detected by visual yellow–orange–brown colors development, and by UV–Vis spectroscopy.

2.4. Synthesis of [Fe(III)(Cl)(pdc)(H_2O)(DMSO)] *1*

Equimolar amounts of iron (0.00821 g, 0.147 mmol), pyridyn-2,6-dicarbonylodichloro ligand (pcd, 0.0303 g, 0.147 mmol) and DMSO (1.5 mL) were placed in a flask and the mixture was kept under N_2 atmosphere and magnetic stirring at 80 °C for 2.5 h. Green light crystals were filtered off, and dried under vacuum. The reaction yield 81% of **1**, based on the isolated pure product was obtained. Mp: 228–230 °C; UV–Vis $\lambda_{max}/\varepsilon$ ($CHCl_3$) nm/M^{-1} cm^{-1}: 205/36,700, 209/38,600, 211/39,500, 216/38,600, 741/100, 836/100 and 970/1600; IR υ_{max} (KBr cm^{-1}): 1631.7(s) (C═O), 1029.9(s) (S═O), 476.4(s) (Fe—N), 439.8(s) and 686.7 (Fe—O), 418.5(s) (Fe—Cl); ^{1}H NMR (ppm): 62.2, 54.58, 49.35, 40.00, 18.56, 13.40, 3.00, 2.30, 1.88, −9.32, −10.93; powder sample ESR: 300/77 (K) $g_1 = 11.909/9.992$, $g_2 = 4.139/4.036$, $g_3 = 2.944/2.805$, $g_4 = 2.197/2.196$, $g_5 = 2.004/-$; $\chi_M T = 0.318$ emu mol^{-1} K rt; HRMS (FAB+) calcd. for $C_9H_{11}ClFeNO_6S$ [M+H$^+$]: 352.55, found: 352.

3. Results and discussion

3.1. Synthesis

Direct synthesis method [16–18] and traditional method [21,24] using the same transition metals with zero oxidation state or their salts, respectively, can produce different and/or similar compounds. The control of the reaction conditions (temperature, reaction time and solvent) allows isolating the compounds obtained during the direct synthesis without salts as polluter. In this work we have isolated, by direct synthesis, one pure product, **1**, making to react Fe(0) with pcd ligand which has been studied by electronic and magnetic spectroscopy. These results have been correlated with the **1** structure.

3.2. Crystal structure

The asymmetric unit of **1** consists of four monomeric units [Fe(III)(Cl)(pdc)(H_2O)(DMSO)] with equal geometries. The iron(III) ion shows local geometry better described as distorted octahedral (Fig. 1), showing totally different angles and bond lengths around the iron ion in the plane O(3), N(1), O(4), Cl(1). Axially the iron ion shows an asymmetric coordination with O(2) atom of DMSO

Table 2
ESR Fe^{III} species for **1** present in (a and b) as powder samples at 300 and 77 K; (c–f) in methanol solution at 77 K.

	Species A cluster	Species B Species C High spin $S = 5/2$			Species D Species E qms $S = 3/2, 5/2$		Species F Low spin $S = 1/2$		
	g	g_1	g_2	g_3	$g_{\|\|}$	$g_\perp$	g_1	g_2	g_3
(a)	11.910	–	–	–	–	–	22.944	2.198	–
					4.139	–			
(b)	10.200	–	–	–	–	–	22.571	2.286	–
					4.277	–			
(c)	10.898	–	–	–	–	–	22.847	2.481	–
					3.705	–			
(d)	–	8.540	4.154	–	5.226	–	32.726	2.399	2.524
		8.023	4.154	–	4.758	–			
(e)	–	9.023	4.444	–	6.410	–	32.719	2.612	2.336
		7.936	4.444	–	5.136	–			
(f)	–	8.058	4.286	–	5.573	–	33.538	2.970	2.540
		7.237	4.286	–	4.788	–			

and O(1) atom of water. The pdc ligand contains aromatic groups that keep to the iron ion into a quasi-planar square through with three coordination bonds to two oxygen atoms and one nitrogen atom of the pyridine-pdc ligand forming two chelato rings. A long fourth coordination in the same plane is established with the chloro ion. The equatorial plane that contains O(3), N(1), O(4) and Fe(1) is distorted, the r.m.s. deviation from a least-squares plane containing these atoms is 0.0056 Å, the iron ion deviation is 0.017 Å.

As expected for this molecule, the electron density of the carboxylatos oxygen atoms of the pdc ligand and the covalence of the oxygen atoms towards Fe(III) is asymmetric (Table 1).

The equatorial plane that contains O(3), N(1), O(4) and Fe(1) is distorted, the r.m.s. deviation from a least-squares plane containing these atoms is 0.0056 Å, the iron ion deviation is 0.017 Å. Molecules pack as planes along the short *b*-axis (Fig. 2a) and forming step-layers of molecules, the normal to these layers are 45° sloped from the *c*-axis. The molecules are in alternating layers parallel orientation, which are in layer with the molecules showing their chloro ligands in front to the next molecules step-layer (Fig. 2a). The packing index for **1** is 68.5% and no interstitial solvent molecules are observed in crystal structure. The crystalline structure of **1** shows polar interaction in *x*, *y*, *z* directions, yielding a supramolecular structure (Fig. 2a). Important distances in the molecular structure are: O5—H1b 1.868 Å, O4—H1b 3.951 Å, O6—H1a 1.871 Å and O3—H1a 2.903 Å, which suggest possible magnetic pathways no direct Fe···Fe (Fig. 2b). However, the angle O5—H1b—O1 (144.7°), O6—H1a—O1 (165.48°) are characteristic of antiferromagnetic interactions [25,26] (Fig. 2b). Other possibilities, in the same Fig. 2, are the distance O4—O1 and distance O2—O1 (4.572 Å and 3.461 Å, respectively, with angles Fe1—O4—O1 of 130.37° (Fe1 in left molecule), O4—O1—Fe1 of 99.02° Fe1 in middle molecule) and Fe1—O2—O1 of 161.68° (Fe1 in right molecule), Fe1—O1—O2 of 115.29° (Fe1 in middle molecule). Newly, in general, with exception of the 99.02°, these angles correspond to antiferromagnetic interaction Fe—Fe [25,26]. The Fe···Fe interaction pathways can propose through of chains of proximately nine atoms (~9 Å), or directly Fe—Fe through of space at the shortest distance of 6.461 Å (Fig. 2b), implying always a weak antiferromagnetic interactions.

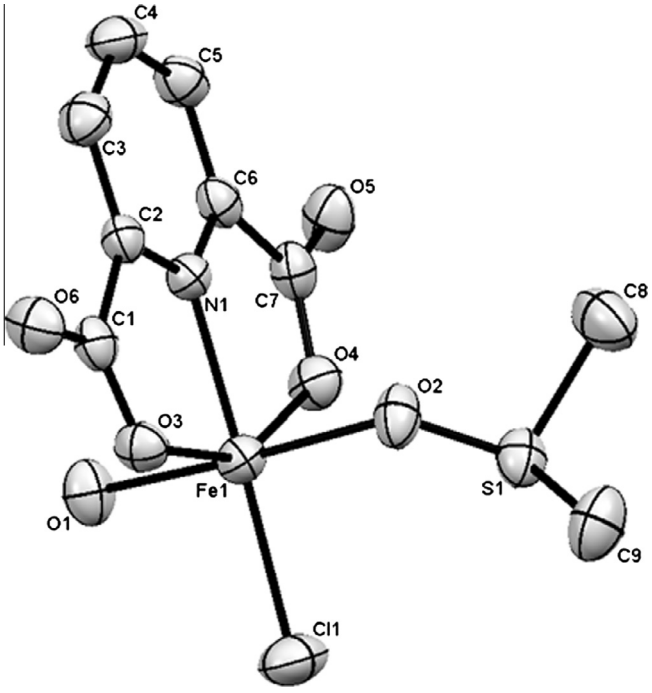

Fig. 1. Molecular structure with displacement ellipsoids at the 30% probability level.

3.3. UV/Vis and NIR spectroscopy

The UV/Vis/NIR spectrum of **1** (Fig. 3) shows a band which contains four peaks at $\lambda_{max}/\varepsilon$ (nm/M^{-1} cm^{-1}) = 205/36,700, 209/38,600, 211/39,500, and 216/38,600 of $\pi \rightarrow \pi^*$ transitions mixed with vibrations characteristic of pyridine group. $\lambda_{max}/\varepsilon$ (nm/M^{-1} cm^{-1}) = 255/17,000 belongs to the $n \rightarrow \pi^*$ transitions. At 279/13,420 are observed transfer charge transitions $d \rightarrow \pi^*$. Asymmetric broad and short bands at $\lambda_{max}/\varepsilon$ (nm/M^{-1} cm^{-1}) at 741/100, 836/100 and 970/1600, corresponding to d_{xz}, $d_{yz} \rightarrow d_x2_{-y}2$, $d_{xy} \rightarrow d_x2_{-y}2$, and $d_z2 \rightarrow d_x2_{-y}2$, transitions, which are detected under higher concentration by amplification of their experimental detection, informs us about the presence of a strongly distorted octahedral ligand field surrounding the iron ion [27,28]. The UV–Vis results if **1** is in full agreement with the X-ray structure determination.

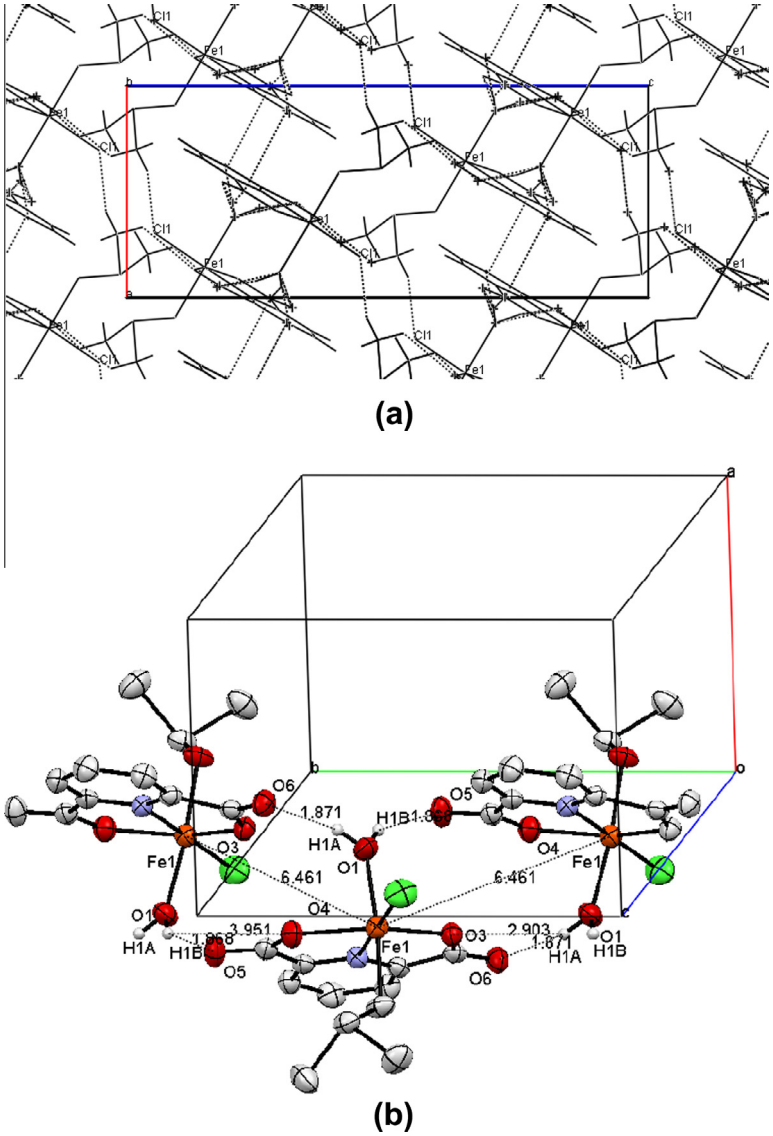

Fig. 2. (a) The packing structure of **1** viewed along the *b* axis of the monoclinic cell. Supramolecular arrangement of **1** showing interactions in *x*, *y*, z, directions; (b) possible interacting magnetic pathways Fe^{III} ions through O(5)···H(1B), H(1A)···O(6) atoms (1.868 Å, 1.871 Å, respectively); O4···H1B, O3···H1A atoms (3.951 Å, 2.903 Å, respectively); shortest constant distances between Fe(III) ions (6.461 Å). Unit cell axes *a*, *b*, *c*.

Middle IR spectrum of **1** shows the characteristic functional group vibration υ_{O-H} at 3440.9, 3103.3, 3006.9; υ_{C-H} at 2927.8, 2862.2 cm^{-1}; υ_{C-O} at 1076.2 cm^{-1}. Far IR shows υ_{Fe-O} at 686.6, 439.8 cm^{-1}, υ_{Fe-N} at 476.4 cm^{-1} and υ_{Fe-Cl} at 418.5 cm^{-1} [29,30] (Fig. SI1).

3.4. ^{1}H NMR spectroscopy

The ^{1}H NMR spectrum of **1** shows line broadening due to two processes: (a) dipolar relaxation of nearest ligand nucleus to the metal, and (b) Fermi contact to nearest neighbor ligand nucleus. Operation of both processes allows efficient relaxation of the proton nuclei [31–33]. Hence, it is not possible to assign the isotropic chemical shifts and to quantify the protons present (Fig. SI2).

3.5. Magnetic behavior

Magnetic susceptibility of a powdered sample of **1** in the form χ_M versus temperature is showed in Fig. 4a and b. The Curie–Weiss law analysis, characteristic of paramagnetic behavior, yields θ values of −0.803 K, with *g* values of 1.89, which suggests the presence of a weak antiferromagnetic exchange coupling interaction [34–36]. The susceptibility data are fitted to antiferromagnetic Heisenberg Hamiltonian, $H_{ex} = -2JS_1 \cdot S_2$, for a pair of exchange-coupled $S = ½$ ions using different equations [34–37]. The best fit for Eq. (1) [36] gives a *g* value of 1.81 and a constant exchange interaction value of $J = -1.803$ cm^{-1} (Fig. 4a). For Eq. (2) [36] the best fit gives a *g* value of 1.832, and a constant exchange interaction value of $J = -1.102$ cm^{-1} (Fig. 4b).

$$M = [Ng\beta \sinh(g\beta H/kT)]/[\exp(-2J/kT) + 2\cosh(g\beta H/kT) + 1] \quad (1)$$

$$\chi_M = [N\beta^2 g^2/3k(T-\theta)][1 + (1/3)(\exp(-2J/kT)]^{-1}(1-\rho) + [(N\beta^2 g^2)\rho]/4kT + N\alpha \quad (2)$$

The terms in Eqs. (1) and (2) have the usual meanings [34–38].

In crystal structure section, it was shown that the shortest distance between two iron ions is 6.461 Å, and the Fe—Fe magnetic

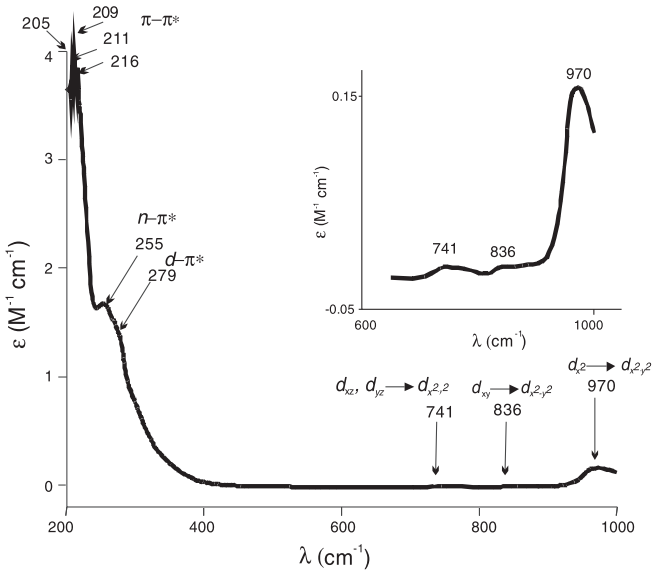

Fig. 3. UV–Vis spectrum of **1** methanol solution.

pathways may be through of different atom chains. In addition, some of this chain contains carbon atoms with no unpaired electrons. For all these atomic features, it could be expected a weak exchange interaction, as is obtained in the magnetic measurement.

3.6. ESR spectroscopy

The X-band ESR spectra of a powdered sample of **1** were recorded at 300 and 77 K. The powder sample of **1** shows an absorption, which is typical of iron ferromagnetic absorptions [39,40], at fields as low as 56.705 mT at 300 K and at $H = 64.530$ mT at 77 K (Fig. 5a and b). This absorption shows a shifts of the order of 7.825 mT when the temperature is lowered from 300 K to 77 K. This resonance field shift is due to the increase of the internal magnetic field that each iron ion is experiencing due to the magnetic ordering of the rest of magnetic atoms. It should be noted that the existence of an internal magnetic field is only compatible with ferro – or ferri – magnetic order. And this in turn is compatible with the squid magnetic measurements and the structure discussed [41].

Fig. 5c–f shows the spectra of **1** in methanol solution at different concentrations and at 77 K. It is clearly visible the development of different species of Fe(III) when concentration is lowered. It is surprising in Fig. 5c to observe clearly the same spectrum as in the polycrystalline solid.

The ferromagnetic order is preserved from the solid sample. We believe that the supramolecular structure of **1** is breaking apart as "big blocks" that each one preserves the magnetic characteristics of a whole crystallite. Both spectra show characteristic powder ferromagnetic resonances [39,40].

When concentration is lowered at 26 mM appears several Fe(III) species: rhombic, high spin $S = {}^5/_2$ and low spin $S = {}^1/_2$, and qms $S = {}^5/_2$, $S = {}^3/_2$, in accord with all exchange of ligands present in solution. These species are present at concentration as low as 5 mM.

The ESR spectra in Fig. 5c–f are very similar to some ferric hemeproteins and porphyrin–Fe(III)-complexes spectra reported as model compounds of peroxidase enzymes [1–7,9–11,43]. Table 2 contains the ESR information of **1** in solution. The spectra identified correspond at Fe(III) species as follow: two high spin species, $S = {}^5/_2$, with rhombic spectra, two species of spin quantum mixed,

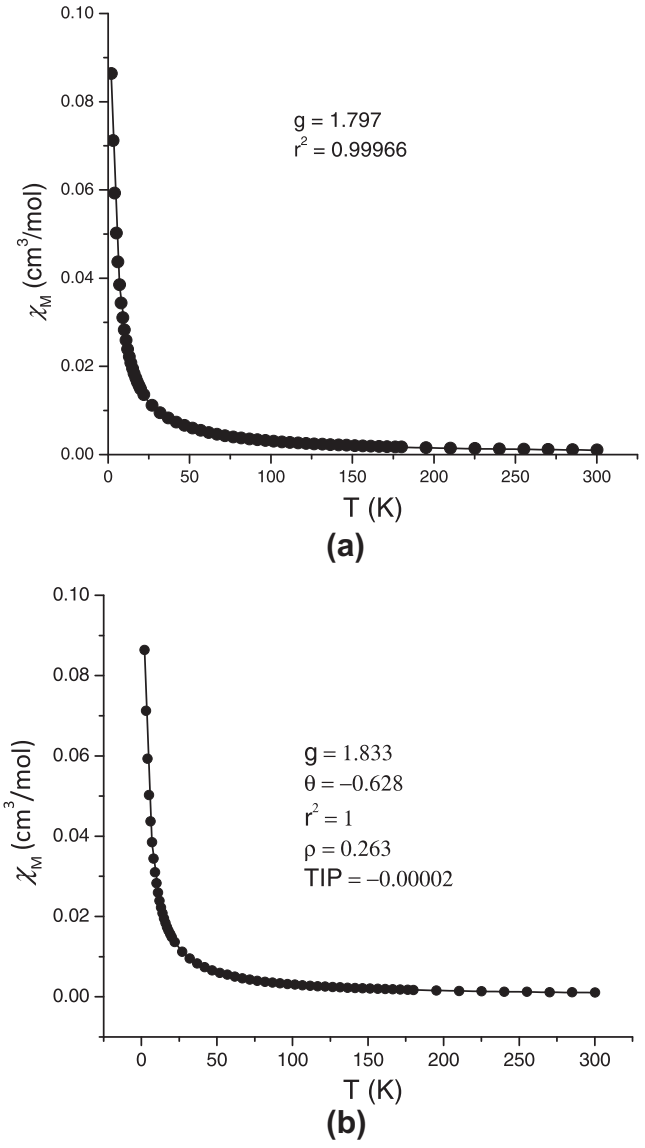

Fig. 4. χ_M vs. T of **1**. The solid line corresponds to the theoretical fit of Eqs. (1) and (2) for the experimental data. The model includes a weak antiferromagnetic behavior. The best fits give: (a) $J = -1.803$ cm^{-1} and (b) $J = -1.102$ cm^{-1}.

$S = {}^5/_2$, $S = {}^3/_2$, with axial spectra, and one low spin species, $S = {}^1/_2$, with a rhombic spectrum [1–7,9–11,43].

At down field are observed two signals with g values between 7 and 9 (B, C) and one signal with g value ~4.29 corresponding to high spin state of iron(III) with rhombic spectra, characteristic of octahedral geometries strongly distorted, with the zero field splitting parameters D and E are no zero (Fig. 5d and e spectra and Table 2(d) and (e) data) [33,41,42,44]. The third signals corresponding at these rhombic species are not clear in Fig. 5 ($g \sim 1.7$–1.5). These rhombic species of high spin (in low proportion) must correspond to **1** with DMSO ligand replace for CH_3OH, Cl^- or H_2O in all possible combinations, producing a weak ligand field, a high spin and a large deviation from octahedral symmetry. At up field it is possible to observe three signals with g values $g \sim 2$, which are typical of low spin, $S = {}^1/_2$, and of a rhombic spectrum. This specie of Fe(III) is in low proportion and corresponds at the Fe(III) ion in a strong ligand field [3,4,9,43]. Finally, the middle field signals, with g values $4 > g < 6$ have been reported as species with qms and axial spectra [1–7,9,43]. These species are in higher

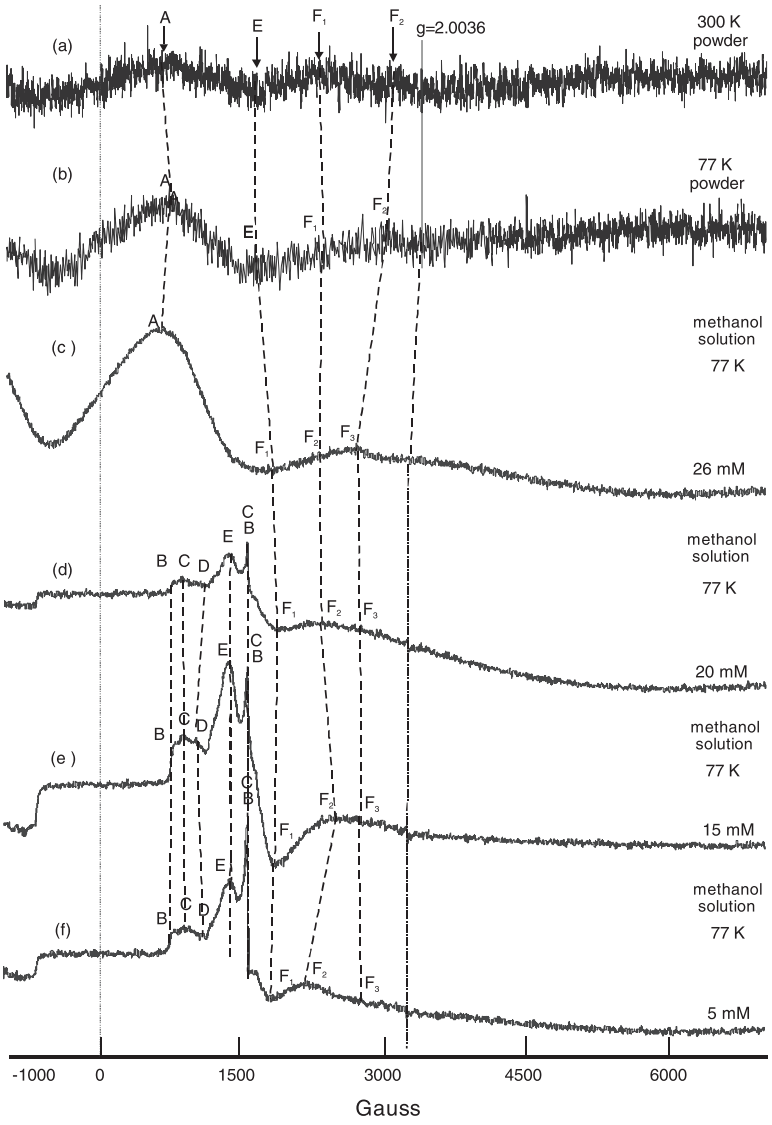

Fig. 5. (a and b) ESR powder spectra for **1** at 77 K and at 300 K, (c–f) ESR methanol solution at different concentrations and at 77 K. From −1000 G to 7000 G field.

proportion. When the sample at ca 15 mM was recorded from 160 K to 77 K the same species of Fe(III) were detected with very little change of their *g*-values. This is also a sign of the paramagnetic character of these signals, and it informs us that the spin state mixture of the Fe(III) is not dependent on temperature variation. The qms of Fe(III), which is different from thermal spin equilibrium, is the quantum mechanical mixing of some quartet state, $^4A_2$ into the sextet $^6A_1$ [1–4]. Maltempo [1–3] has shown that this mix is the only quantum mechanical mixing [2], which have been observed in octahedral compounds, where the square planar size is reduced in function that the coordination Fe(III)-ligand is stronger that the axial coordination. In consequence, rise the energy of $d_x2_{-y}2$ orbital atomic and low the energy of the d_z2 orbital atomic, favoring a high spin $^5/_2$ mixed with the $^3/_2$ spin state, $4 > g < 6$ (Fig. 6).

It should be noted that our ESR spectrometer equipped with a zero-cross unit is able to register the ESR feature "B" at negative fields, mirror image-inverted from the B-signal at positive fields, Fig. 5, confirming the paramagnetic nature of these resonances [44].

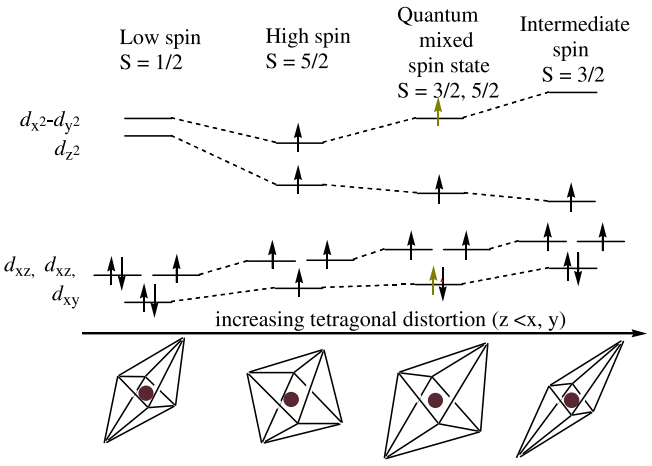

Fig. 6. Different spin states of Fe^{III} and their respective octahedral geometry distorted.

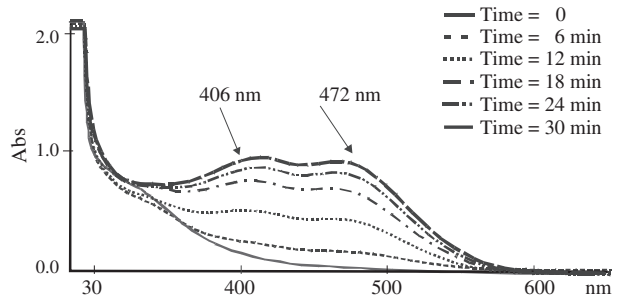

Fig. 7. The characteristic UV–Vis bands corresponding at the POG appear and growth when **1** is used as catalyst in the guaiacol test, which is characteristic of peroxidase enzymes. Catalytic activity decreases notably at $t > 30$ min to initiate the catalytic activity.

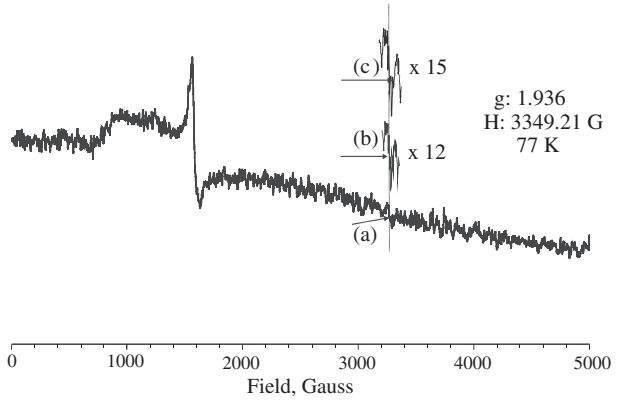

Fig. 8. ESR spectra of the guaiacol + H_2O_2 + **1** reaction, observing the radical signal characteristic of Compound I, π-radical-cationic ferryl, intermediate oxidant: (a) at $t = 36$ min (1 accumulation); (b) inset, at $t = 40$ min (4 accumulations); (c) inset, at $t = 52$ min (8 accumulations). The g values are the same at different times and the slow sweep time is of 3 min for each accumulation.

*3.7. Catalytic activity of **1***

Determination of guaiacol oxidation with hydrogen peroxide using **1** as catalyst is carried out as previously described for horseradish peroxidase and other reports [1,2,10,20]. Formation of POG is achieved by observation visual of the yellow–orange–brown colors development, which is typical of the qualitative test for peroxidase enzymes [20]. The same guaiacol test is followed by UV–Vis spectroscopy observing the increase of the bands at $\lambda_{max} \sim 410.6$ and 462.8 nm, characteristic of POG (Fig. 7). The optimum final concentrations for this guaiacol test are: guaiacol 6 mM, hydrogen peroxide 2.8 mM and **1** 3 mM. Other possible reactions which are ruled out: (a) **1** + guaiacol → nothing; (b) guaiacol + H_2O_2 → nothing; (c) **1** + H_2O_2 → nothing. Only when hydrogen peroxide, guaiacol and **1** are mixed the guaiacol test is possible. The last test is recorded by ESR spectroscopy at 77 K [Fig. 8], and it is possible to observe at $H = 3379.21$ G with g value of 1.936 the characteristic signal corresponding to the radical π-cationic-radical ferryl, Compound **I**, intermediate compound formed during the catalytic activity of peroxidase enzymes [43].

4. Conclusions

The Fe(III) ions lie at the center of a distorted octahedral geometry which is consistent with the UV/VIS spectrum of **1** showing three broad and very small bands which correspond to *d–d* transitions, characteristic of a low symmetry Fe(III) high spin species. Magnetization versus temperature studies of **1** gives a Fe···Fe weak magnetic behavior which is fully compatible with possible magnetic pathways, through of N, O, and H atoms-bridges making angles typical of antiferromagnetic interaction. The shortest distance Fe—Fe ions is of 6.461 Å, and this also implies a weak exchange interaction through space. ESR spectra of polycrystalline powder sample of **1** at 300 K and 77 K, show strong magnetic interaction dominant, which disappears at ca < 26 mM by magnetic exchange and an increase in internal field of ~3.58 mT when the temperature is lowered from 300 K to 77 K. In methanol solution at the highest concentration ca 26 mM, the supramolecular structure has not been destroyed yet and "big-block" clusters prevail in the frozen concentrated solution. At concentrations ⩽20 mM new signals emerge clearly. No signs of the FMR signal remain. A full new spectrum emerges, showing Fe(III) species with high spin, low spin, and qms, characteristic of bio-molecules with iron-porphyrin active sites. The correlation between the qms of iron(III) in solution by ESR spectroscopy with the catalytic activity as peroxidase enzymes shown for **1**, is demonstrated in this study.

Acknowledgment

The present work has been supported by Vicerrectoría de Investigación y Estudios de Posgrado from BUAP, Divulgation of Science, 2009–2010.

Appendix A. Supplementary material

Supplementary data associated with this article can be found, in the online version, at http://dx.doi.org/10.1016/j.molstruc.2013.02.021.

References

[1] M.M. Maltempo, T.H. Moss, M.A. Cusanovich, Biochim. Biophys. Acta 342 (1974) 290–305.
[2] M.M. Maltempo, T.H. Moss, Q. Rev. Biophys. 9 (1976) 181–215.
[3] J.C.A. Reed, T. Mashiko, S.P.W. Bentley, M.E. Kastner, W.R. Scheidt, K. Spartalian, G. Lang, J. Am. Chem. Soc. 101 (1979) 2948–2958.
[4] C.A. Reed, F. Guiset, J. Am. Chem. Soc. 118 (1996) 3281–3286.
[5] A. Gismelseed, E.L. Bominaar, E. Bill, A.X. Trautwein, H. Winkler, H. Nasri, P. Dopelt, D. Mandon, J. Fisher, R. Weiss, Inorg. Chem. 29 (1990) 2741–2749.
[6] D.R. Evans, C.A. Reed, J. Am. Chem. Soc. 122 (2000) 4460–4467.
[7] G.P. Gupta, G. Lang, Y.J. Lee, R. Scheidt, K. Shelly, C.A. Reed, Inorg. Chem. 26 (1987) 3022–3030.
[8] A. Ogoshi, H. Sugimoto, Z. Yoshida, Biochim. Biophys. Acta 621 (1980) 19–28.
[9] Sánchez-Sandoval, D. Ramírez-Rosales, R. Zamorano-Ulloa, C. Álvarez-Toledano, M. Moya-Palencia, Y. Reyes-Ortega, J. Biophys. Chem. 106 (2003) 253–265.
[10] T.G. Traylor, W.A. Lee, D.V. Stynes, J. Am. Chem. Soc. 106 (1984) 755–764.
[11] Y. Reyes-Ortega, C. Álvarez-Toledano, D. Ramírez-Rosales, A. Sánchez-Sandoval, E. González-Vergara, R. Zamorano-Ulloa, J. Chem. Soc., Dalton Trans. (1998) 667–674.
[12] M. Stuart, J. Chem. Theory Comput. 4 (2008) 2057–3066.
[13] M. Bühl, H. Kabrede, J. Chem. Theory Comput. 2 (2006) 1282–1290.
[14] W.-G. Han, T. Lovell, T. Liu, L. Noodleman, Inorg. Chem. 43 (2004) 613–621.
[15] M. Reiher, Inorg. Chem. 41 (2002) 6928–6935.
[16] Chen, S.-M. Peng, J. Am. Chem. Soc. 119 (1997) 2563–2569.
[17] R. Gutiérrez, J. Vázquez, R.A. Vázquez, Y. Reyes, R.A. Toscano, M. Martínez, C. Álvarez, J. Coord. Chem. 5 (2001) 313–321.
[18] D. Garnovskii, B.I. Kharisov, G. Gojon-Zorrilla, D.A. Russ Garnovskii, Chem. Rev. 64 (1995) 201–221.
[19] Y. Reyes-Ortega, J.L. Alcántara-Flores, M.C. Hernández-Galindo, D. Ramírez-Rosales, S. Bernès, J.C. Ramírez-García, R. Zamorano-Ulloa, R. Escudero, J. Am. Chem. Soc. 127 (2005) 16312–16317.
[20] H.U. Bergmeyer (Ed.), Methods of Enzymatic Analysis, Academic Press, New York, 1874. p. 494.
[21] M. Rafizadeh, B. Mehrabi, V. Amani, Acta Crystallogr. E62 (2006) 332–334.
[22] XSCAnS Users Manual, Release 2.21, Siemens Analytical X-ray Instruments Inc., Madison, WI, USA, 1996.
[23] SHELXTL-Plus, Release 5.10, Siemens Analytical X-ray Instruments Inc., Madison, WI, USA, 1997.
[24] E.E. Sileo, G. Rigotti, B.E. Rivero, M.A. Blesa, J. Phys. Chem. Solids 58 (1997) 1127.
[25] R.D. Willet, D. Gateschi, O. Khan (Eds.), Magneto-Structural Correlations in Exchange Coupled Systems, Reidel, Dordrecht, The Netherlands, 1985.
[26] Olivier Kahn, Molecular Magnetism, VCH Publisher, USA, 1993.

[27] S. Tanase, M. van Son, G.A. van albada, R. de Gelder, E. Bouwman, J. Reedijk, Polyhedron 25 (2006) 2967–2975.
[28] S. Roy, T.N. Mandal, A.K. Barik, S. Pal, S. Gupta, A. Hazra, R.J. Butcher, A.D. Hunter, M. Zeller, S.K. Kar, Polyhedron 26 (2007) 2603–2611.
[29] Z.E. Koc, I. Ucan, Trans. Metal Chem. 32 (2007) 597–602.
[30] N. Nishat, K.A. Siddiqi, Sh.A.A. Nami, A. Umar, Synth. React. Inorg. Metal-Org. Chem. 34 (2004) 145–161.
[31] L.B. Dugad, S. Mitra, Proc. Indian Acad. Sci. Chem. Sci. 93 (1984) 295–311.
[32] I. Bertini, S. Ciurli, A. Dikiy, R. Gasanov, C. Luchinat, G. Martini, N. Safarov, J. Am. Chem. Soc. 121 (1999) 2037–2046.
[33] R.S. Drago, Physical Methods for Chemists, 2a. ed., Saunders College Publishing, EUA, 1992.
[34] C. Díaz, J. Ribas, M.S. El Fallah, X. Solans, M. Font-Bardía, Inorg. Chim. Acta 312 (2001) 1–6.
[35] W.E. Hatfield, J.A. Barnes, D.Y. Jeter, R. Whyman, E.R. Jones Jr., J. Am. Chem. Soc. 92 (1970) 4982–4984.
[36] B.E. Myers, L. Berger, S.A. Friedberg, J. Appl. Phys. 40 (1969) 1149–1151.
[37] W.E. Marsh, K.C. Patel, W.E. Hatfield, D.J. Hodgson, Inorg. Chem. 22 (1983) 511–515.
[38] S.S. Tandon, L. Chen, L.K. Thompson, J.N. Bridson, Inorg. Chem. 33 (1994) 490–497.
[39] K.K. Andersson, P.P. Schmidt, B. Katterle, K.R. Strand, A.E. Palmer, S.-K. Lee, E.I. Solomon, A. Gräslund, A.-L. Barra, J. Biol. Inorg. Chem. 8 (2003) 235–247.
[40] L.F. Jones, E.K. Brechin, D. Collison, M. Helliwell, T. Mallah, S. Piligkos, G. Rajaraman, W. Wernsdorfer, Inorg. Chem. 42 (2003) 6601–6603.
[41] G. Feher, Electron Paramagnetic Resonance with Applications to Selected Problems in Biology, Gordon and Breach, Science Publishers, New York, 1970.
[42] W. Weltner Jr., Magnetic Atoms and Molecules, Dover Publications, Inc., EUA, 1983.
[43] F.A. Walker, The Porphyrins Handbook, Academic Press, USA, 1999. pp. 81–175.
[44] A. Abragam, B. Bleaney, Electron Paramagnetic Resonance of Transitionions, Oxford University Press, Oxford, England, 1970. p. 700.